UNIVERSITY OF CENTRAL OKLAHOMA

MASTER'S THESIS

Computational Study of Interactions Between DNA Bases and Single-Layer Ti_3C_2 MXene

---

Author:
Michael A. WALKUP

Chair of Committee:
Dr. Benjamin TAYO

Committee Members:
Dr. Gang XU
Dr. Sezin KADIOGLU

Director of School of Engineering:
Dr. Evan LEMLEY

Submitted to the Jackson College of Graduate Studies of the University of Central Oklahoma in fulfillment of the requirements for the degree of Master of Science in the School of Engineering

May 11, 2023

UNIVERSITY OF CENTRAL OKLAHOMA

MASTER'S THESIS

Computational Study of Interactions Between DNA Bases and Single-Layer Ti_3C_2 MXene

Jackson College of Graduate Studies
at the University of Central Oklahoma

A thesis approved for

Michael A. WALKUP

by

Dr. Benjamin TAYO
benjamin tayo

Dr. Gang XU
Gang Xu Digitally signed by Gang Xu DN: cn=Gang Xu, o, ou, email=gxu@uco.edu, c=US Date: 2023.05.08 19:26:21 -05'00'

Dr. Sezin KADIOGLU

May 8, 2023

UNIVERSITY OF CENTRAL OKLAHOMA

Abstract

School of Engineering

Master of Science

Computational Study of Interactions Between DNA Bases and Single-Layer Ti_3C_2 MXene

by Michael A. WALKUP

Electronic DNA sequencing using atomically thin 2D-based nanodevices has recently emerged as the next-generation of DNA sequencing technology. Recent molecular dynamics simulations showed that single-layer Titanium Carbide (Ti_3C_2) has a great potential for detecting individual DNA bases. In this work, we employ first-principles techniques based on density functional theory (DFT) to quantify the electronic interactions between the four DNA nucleobases (adenine, thymine, guanine, and cytosine) with 2D Ti_3C_2. Our results showed two distinct interaction mechanisms between DNA nucleobases and Ti_3C_2, namely, physisorption and chemisorption. Unlike graphene, where the binding energy for physisorption of DNA nucleobases is about 0.5 eV, we observe that the binding energy for physisorption for Ti_3C_2 is around 0.1 eV. This difference correlates to an increased distance between the nucleobases and the Ti_3C_2 ($\sim$5.6 Å) compared to graphene ($\sim$3.1 Å), indicating a weaker interaction. Based on these results, other electronic detection mechanisms, such as nanopore sequencing, would be worth exploring for Ti_3C_2.

Acknowledgements

First and foremost, I would like to thank Dr. Benjamin Tayo for his guidance and mentorship throughout my entire time performing research at the University of Central Oklahoma. I also greatly appreciate the assistance of everyone I encountered in the Department of Engineering and Physics, particularly Dr. Evan Lemley for his work in the High Performance Computing Center and especially Kimberly Webb for her assistance with my course schedules and paperwork. I would also like to thank my committee members Dr. Tayo, Dr. Gang Xu, and Dr. Sezin Kadioglu for their time and patience. Lastly, I cannot express enough gratitude for my family and friends who supported me to pursue my academic career.

Contents

List of Figures

List of Tables

List of Abbreviations

List of Abbreviations

2D	Two-dimensional
3D	Three-dimensional
BYLP	Becke-Lee-Yang-Parr
CPU	Central Processing Unit
DFT	Density Functional Theory
DNA	Deoxyribonucleic Acid
DOS	Density of States
GGA	Generalized Gradient Approximation
GNP	Graphene Nanopore
GNR	Graphene Nanoribbon
GO	Geometry Optimization
NERSC	National Energy Research Supercomputing Center
PBE	Perdew-Burke-Ernzerhoff
PWscf	Plane-Wave Self-Consistent Field
SCF	Self Consistent Field
SE	Schrodinger Equation
SLURM	Simple Linux Utility for Resource Management
vdW	van der Waals
VESTA	Visualization for Electronic and Structural Analysis
XYZ File	File containing atomic x, y, and z coordinates in a molecular system

Dedicated to my sister, Mickey, and my parents, John and Zepure. Without their love and support, I would not be where I am today.

Chapter 1

Introduction

In the field of material science, two-dimensional (2D) materials have garnered interest for their applications in biotechnology. One such application, the topic of this thesis, involves using molecular monolayers to detect DNA bases for sequencing [1]. Research into DNA sequencing seeks to optimize the process and make the detection quicker, cheaper, and more accurate through investigating new methods and materials. These methods include the Sanger technique (using DNA polymerase enzyme to generate DNA fragments from single-strand DNA templates [2]), amplification (duplicating DNA bases in a sequence to increase detectability [3]), and nanopore sequencing (measuring electronic interactions when DNA strands are fed through nanometer-scale pores in a 2D material [4]).

While earlier nanopore research investigated the viability of biological structures, more recent research has found promising solid-state devices that could more cost-effectively sequence DNA. Graphene in particular possesses desirable characteristics such as high carrier mobility (how easily electrons can move through the material) [5]. Other studies have investigated the viability of molybdenum disulfide (MoS_2), hexagonal boron nitride (h-BN) [6], and phosphorene [7], with varying levels of success. In nanopore configurations (shown in Fig. 1.1a), the speed of the DNA passing through the nanopore can outpace the temporal resolution of the measurement device, causing inaccurate readings [8]. Instead of using a solid-state nanopore, an alternative method involves adsorption of the DNA base onto a solid-state surface (shown in Fig. 1.1b) and measuring the binding energy of each DNA base [6]. However, a relatively limited number of materials have been tested, and those materials have encountered problems with high physisorption (graphene) or degradation under voltage stress (MoS_2). In this project, we look into evaluating adsorption onto a titanium carbide MXene (Ti_3C_2) surface. Previous studies have shown Ti_3C_2 to be a promising material for this application, as its hydrophilic surface provides better signal performance and stability [6].

To test the viability of Ti_3C_2, this project involves computational methods using density functional theory (DFT) to calculate the binding energies between DNA bases and the MXene surface. We utilized Quantum Espresso (QE) software, namely the PWscf program, to perform calculations on the University of Central Oklahoma's supercomputer, "Buddy", and the National Energy Research Scientific Computing Center

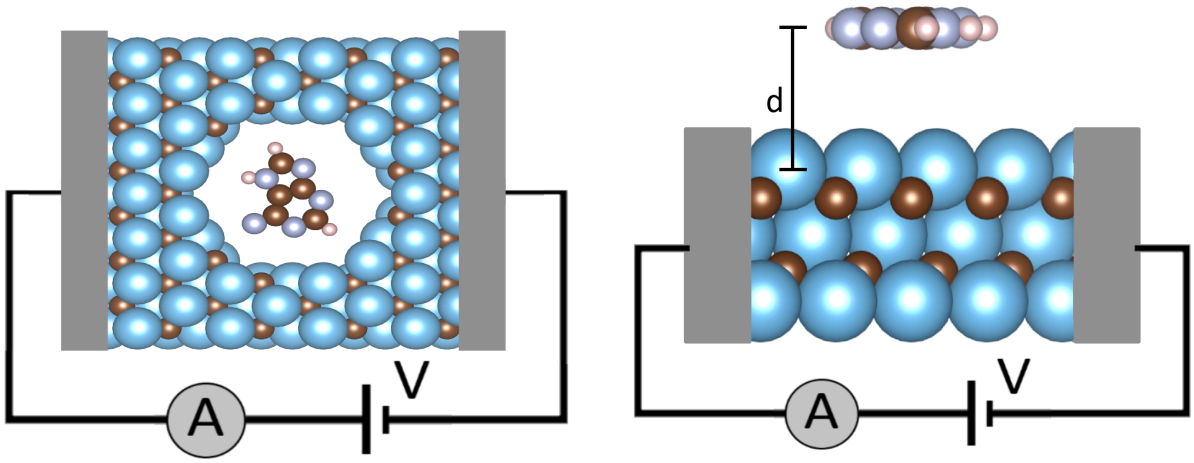

(A) Nanopore (B) Nanoribbon

FIGURE 1.1: Simplified schematics of solid-state DNA sequencing.

(NERSC). To create input files for the molecular systems, Python scripts were written to generate the spatial coordinates of each atom in the system and write the data to XYZ files. All figures displaying atomic structures were generated using VESTA.

Graphene, for its simplicity, will be analyzed prior to Ti_3C_2, both in adsorption configurations. Each system will be evaluated by their binding energies and adsorption heights. Chapter 2 describes DFT and the QE computational process. Chapters 3, 4, and 5 analyze the use of DFT to calculate the electronic properties of DNA nucleobases on their own, adsorbed on graphene, and adsorbed on Ti_3C_2.

Chapter 2

Density Functional Theory

2.1 Background

When dealing with molecular systems that involve large number of atoms, simulating every particle as discrete creates a many-body problem too complex for any computer to perform calculations. To remedy this computation problem, DFT considers the electrons as a density cloud instead of discrete particles, as seen in Fig. 2.1. DFT methods use the density of the system to find the ground state energy and other properties [9]. In this project, we use Quantum Espresso (QE) software, its Plane-Wave Self-Consistent Field (PWscf) program, and the Perdew-Bruke-Ernzerhof (PBE) functional. There are some common functionals to choose from in the family of generalized gradient approximations (GGAs), such as Becke-Lee-Yang-Parr (BYLP), but we chose PBE for its better performance with energy calculations of metallic materials [10].

In DFT, functionals map electron density wave functions (a set of functions) to the total energy of the system (a set of real numbers). PBE achieves this mapping by calculating an exchange-correlation energy, $E_{\mathrm{XC}}^{\mathrm{PBE}}$, defined as the sum of the exchange energy and the correlation energy. The exchange energy arises from the Pauli exclusion principle, which states that identical particles cannot occupy the same quantum state. Therefore, the distance between two electrons increases, which lowers the overall energy of the system. When one electron moves, all other electrons present in the system alter its motion [12]. The correlation energy measures the degree to which the initial electron's motion changes [13]. The exchange-correlation energy is defined as:

$$E_{\mathrm{XC}}^{\mathrm{PBE}} = \int d^3\mathbf{r}\rho(\mathbf{r})\epsilon_{\mathrm{XC}}^{\mathrm{PBE}}\left(r_s(\mathbf{r}), s(\mathbf{r}), \xi(\mathbf{r})\right) \tag{2.1}$$

where ρ represents the electron density, $\epsilon_{\mathrm{XC}}^{\mathrm{PBE}}$ the exchange-correlation energy per particle, $r_s = (4\pi\rho/3)^{(-1/3)}$ the Wigner-Seitz radius (half of the distance between matching nearest-neighboring ions in a lattice), s the reduced density gradient, and $\xi = (\rho_\uparrow - \rho_\downarrow)/\rho$ the spin-polarization. In summary, PBE takes the GGA approach of integrating over the gradient of the electron density and includes the combination of exchange energy and correlation energy functionals [14].

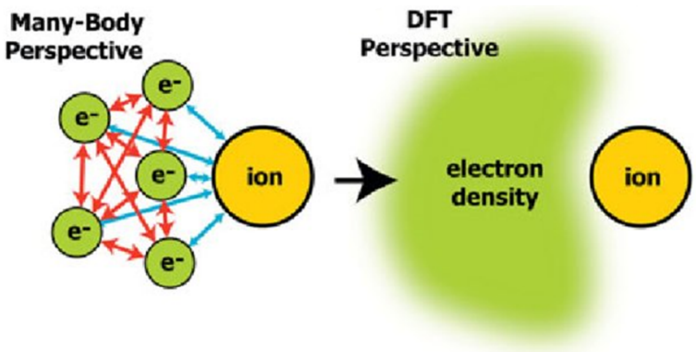

FIGURE 2.1: Qualitative comparison of how atomic systems are treated using molecular dynamics (left) vs. DFT (right) [11].

To determine ρ, we use a self-contained field (SCF) approximation to solve the Schrödinger equation (SE) of the system. The general SCF process starts by guessing the electron density to compute the effective electric potential. Solving the SE using this effective potential energy produces a new electron density. Restarting this series of calculations with the new ρ creates an iterative process, where the system incrementally calculates ρ until the convergence of its value reaches a desired threshold. Now that an optimized electron density is found, QE calculates the total energy of the system and takes the gradient of this result to find the sum of forces acting in the system. If the sum is nonzero, the system does not exist in a ground state. To reach a ground state, the system requires adjusting by way of Geometry Optimization (GO), which changes the positional coordinates of the atoms. QE restarts the SCF calculation using the new system state and will continue repeating the calculations until the sum of forces equals zero, indicating a convergence to a ground state [15]. Fig. 2.2 shows the entire SCF and GO process.

2.2 Input Paramters

In performing DFT calculations, a number of initial parameters have to be set to get a desired result. Input files (.in) categorize input parameters into several blocks, as seen in Appendix A. The following subsections describe key parameters used in each block.

2.2.1 &CONTROL

Settings in the '&CONTROL' block denote basic parameters such as the type of calculation performed. This project mainly utilizes *vc-relax*, *relax*, *scf*, and *bands*:

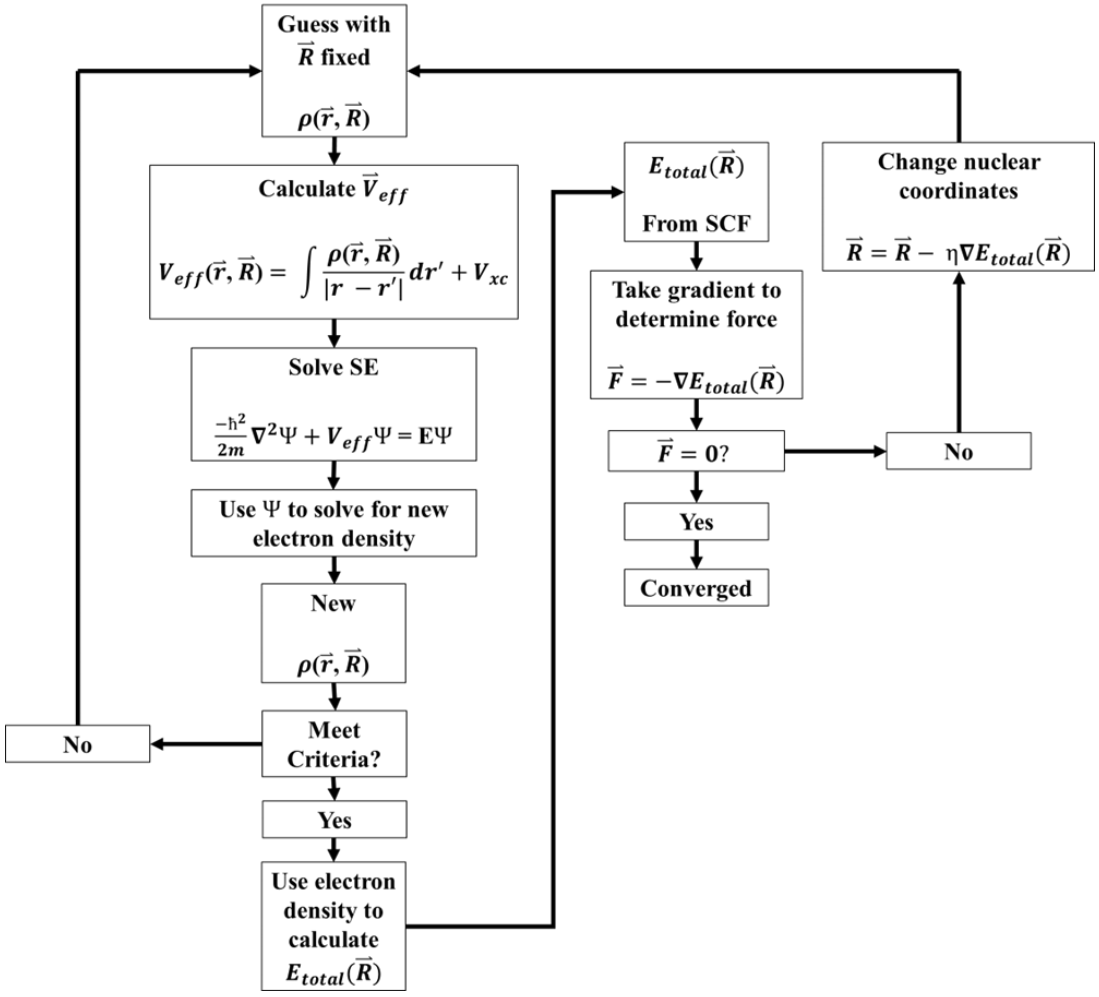

FIGURE 2.2: Flow chart outlining the DFT process [15].

- *vc-relax* ("variable-cell relax") calculates the lowest energy configuration of the molecular structure by allowing the positions of each atom in the system and the size of the unit cell around the system to vary.
- *relax* performs the same calculation as *vc-relax*, but allows the atomic positions to change without altering the unit cell dimensions.
- *scf* consists of the aforementioned SCF calculation and returns the total energy and wavefunction information of the system.
- *bands* takes the wavefunction information provided by the SCF calculation and orders the electron energy bands into a displayable format (band structure).

Energy calculations in this project follow the process of first starting with a *vc-relax* calculation to determine the equilibrium atomic positions and unit cell dimensions of the system. Second, a *relax* calculation freezes the dimensions of the unit cell and allows the atoms in the system to reach a state of minimized total energy. Finally, an *scf* calculation finds the total energy of the system and outputs wavefunction files. To create band structure plots showing the energy levels of electrons in the system, a *bands* calculation takes the wavefunction files and returns data files that can be plotted with a simple Python script.

2.2.2 &SYSTEM

In PWscf, the program performs a Fourier expansion on the electron wavefunctions by utilizing a linear combination of energy plane waves. *ectuwfc* sets the kinetic energy cutoff for these plane waves, limiting the number of plane waves used. Similarly, *ecutrho* sets the energy cutoff for the plane waves used for electronic charge density calculation. The ratio of *ecutwfc* and *ecutrho* determines the point of convergence of energy calculations and is typically set to 1:4, but ultrasoft pseudopotentials (which we use in our calculations) require a lower ratio of around 1:10 [16].

vdw_corr controls whether the calculation includes the effects of the van der Waals (vdW) force in energy calculations. The van der Waals force, separate from electrostatic interactions or bond formations, introduces repulsion/attraction between atoms and molecules in close proximity (on the order of nanometers) [17]. In the computations including the vdW force interactions, the .in file uses the 'Grimme-D2' dispersion energy correction [18]. This correction (Eq. 2.2) multiplies a damping function (Eq. 2.3) and a dispersion coefficient $\left(C_6^{ij} = \sqrt{C_6^i C_6^j}\right)$ and sums across every atom r^{ij} in the unit cell and every translation of the unit cell ($\mathbf{L} = (l_1, l_2, l_3)$). This sum is then multiplied by a global scaling factor s_6, and the damping function also relies on the vdW radii of each atom $\left(R^{ij} = R^i + R^j\right)$. In effect, this factors in atomic interactions that DFT

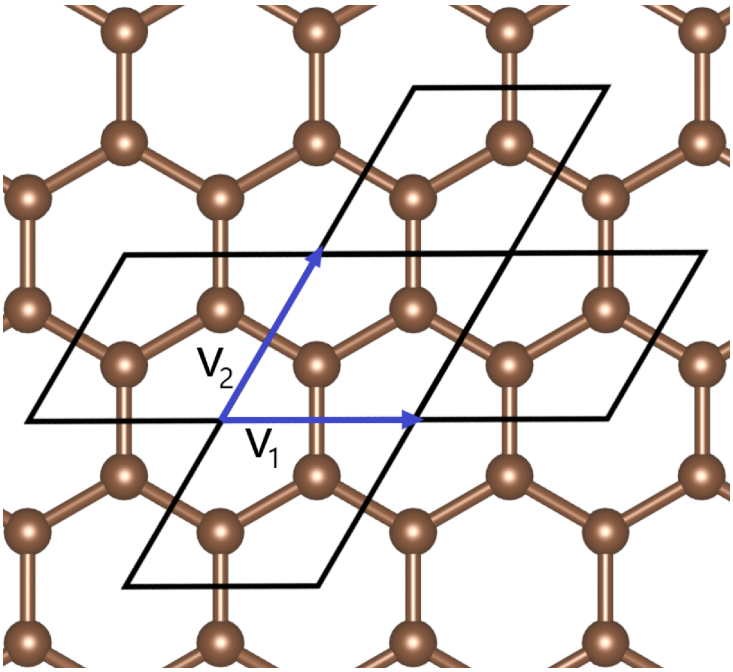

FIGURE 2.3: Graphene example of periodicity used in Quantum Espresso calculations. v_1 and v_2 denote the lattice vectors.

typically does not take into account, affecting the overall energy of the system [19].

$$E_{\text{disp}} = -s_6 \sum_{i=1}^{N} \sum_{j=1}^{N} \sum_{\mathbf{L}}{}' \frac{C_6^{ij}}{r_6^{ij,\mathbf{L}}} f(r^{ij,\mathbf{L}}) \tag{2.2}$$

$$f(r^{ij}) = \frac{1}{1 + e^{-d(r^{ij}/R^{ij}-1)}} \tag{2.3}$$

celldm, the lattice parameter, varies with the size of the system and its crystal structure. To perform DFT calculations, QE requires the lattice structure and its dimensions to repeat the given cell structure as shown in Fig. 2.3. This project analyzes materials with a hexagonal lattice structure, and the lattice vectors v_1 and v_2 equate to $a(1,0,0)$ and $a\left(1/2, \sqrt{2}/3, 0\right)$, respectively, where a equates to the input *celldm(1)* [17].

2.2.3 K_POINTS

This block of parameters sets the sampling resolution of the Brillouin zone used to calculate the energy of the system. These k-points correlate to the critical high-symmetry points of the Brillouin zone, which are shown in Fig. 2.4. For 2D structures, we only

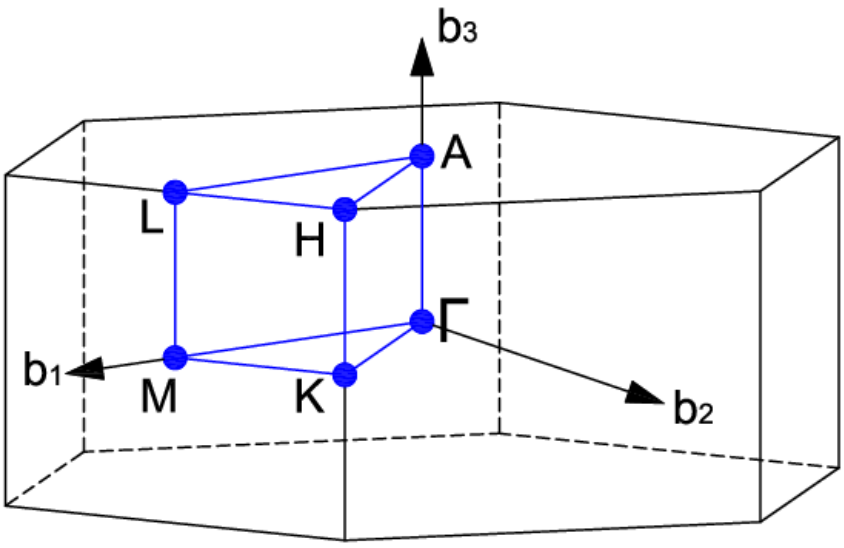

FIGURE 2.4: High-symmetry points of a hexagonal lattice structure [20].

use the Γ-M-K symmetry points. For *vc-relax* and *relax* calculations, we let QE automatically generate the grid of k-points by setting this parameter to:

```
K_POINTS automatic
1 1 1 0 0 0
```

which allows for 1 k-point along each reciprocal lattice vector (“1 1 1") at the center of the Brillouin zone (“0 0 0"). For *scf* calculations, we increase the resolution along the M- and K-axes of the Brillouin zone (“5 5 1") for greater accuracy in energy and band structure calculations.

2.3 Computing with Buddy

In using the Buddy supercomputer, sending a computation job consisted of packaging a script (.sh) file with a .in file and pseudopotential (.UPF) files. The script file manages the settings of the job itself, specifying the number of CPU cores ("nodes"), number of processes the CPUs run in parallel, what program/input files to run, and the location of the output files. My computations utilized 4 nodes and 20 tasks per node. Using Message Passing Interface (‘mpirun’), this file also specifies the input file for running the executable program ‘pw.x’ (plane wave SCF calcualtions) or ‘bands.x’ (electronic bands calculation). Input files contain the aforementioned parameter blocks with the atomic (Cartesian) positional coordinates (‘ATOMIC_POSITIONS’) of each atom in the unit cell, the atomic weights and pseudopotential files of each element (‘ATOMIC_SPECIES’), and the k-point sampling (‘K_POINTS’) of the Brillouin zone.

Buddy, running a SLURM job scheduler, accepts the script file, loads the appropriate programs, and executes the input file. Upon completion of the calculation, Buddy writes the output files to the desired locations and terminates the job.

Chapter 3

DNA Nucleobase Studies Using DFT

3.1 Nucleobase Structure

Genetic information in DNA strands consists of a sequence of four nitrogenous nucleobases: adenine, guanine, cytosine, and thymine. These bases pair up in two groups: purines and pyrimidines. The purines (adenine and guanine) contain a double nitrogen-carbon ring structure, while the pyrimidines (cytosine and thymine) only have one such ring structure. These pairs of nucleobases form bonds in the complete DNA structure, resulting in A-G/G-A and C-T/T-C base pairs [21]. Fig. 3.1 shows the generated structure of each base used in this project, which were acquired from previously completed research by Dr. Tayo.

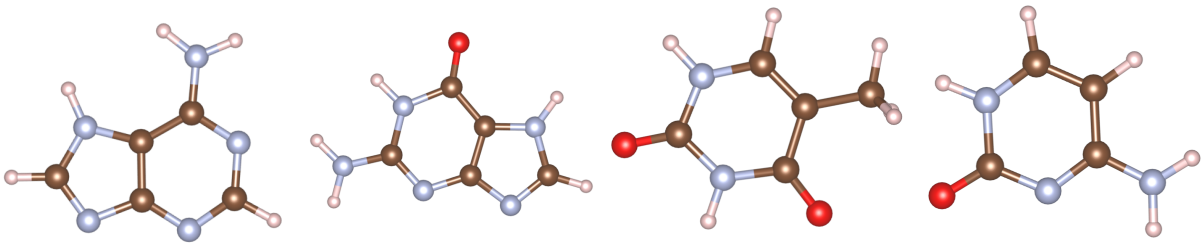

(A) Adenine (B) Guanine (C) Thymine (D) Cytosine

FIGURE 3.1: DNA nucleobase structures: 3.1a & 3.1b make up the purine pair, and 3.1d & 3.1c the pyrimidine pair. Carbon is shown in brown, nitrogen in gray, hydrogen in white, and oxygen in red.

3.2 Creating Nucleobase Input Files

To perform calculations on molecular systems, the positional information of each atom in the system has to be encoded in the input files for Quantum Espresso and VESTA.

Appendix B shows an example XYZ file (which VESTA can use to create a visual representation of the system) contains the number of atoms in the system, a written description, and line-by-line entries of each atom's element and Cartesian positional coordinates. In the process of submitting batch jobs to Buddy, the elements and positional coordinates are copied into the .in file under the '&ATOMIC_POSITIONS' block, such as the one shown in Appendix A.

3.3 Performing Nucleobase Calculations

In the process of calculating the binding interactions between each nucleobase and the adsorption surface, one needs to calculate the total energy of each base. As seen in Eq. 3.1, we find the binding energy by subtracting the total energy of each part of the system (E_{surface} & E_{base}) from the total energy of the system ($E_{\text{surface + base}}$).

$$E_{\text{surface + base}} - (E_{\text{surface}} + E_{\text{base}}) = E_{\text{binding}} \tag{3.1}$$

A *vc-relax* calculation finds optimal positional coordinates and unit cell dimensions, but using the final unit cell dimensions in an additional *relax* calculation further refines the final positions of each atom in the system. Finally, we perform an *scf* calculation to find the total energy (E_{tot}) of each DNA base. In the output file, QE displays these energy values as:

```
!    total energy              =    -174.97723263 Ry
```

where the total energy is given in Rydberg units, which we convert to eV using the conversion 1 Ry = 13.605 693 122 994 eV [22]. This process performed on each nucleobase results in the energy values found in Tab. 3.1.

TABLE 3.1: Total energy of each nucleobase.

Nucleobase	E_{tot} **(eV)**
Adenine	-2316
Guanine	-2758
Thymine	-2380
Cytosine	-2032

Chapter 4

Adsorption of Nucleobases on Graphene

Graphene, consisting of a single layer of carbon atoms, has a simple structure with well-defined properties. This nature of graphene lets the material perform well as a baseline to compare results against and as an introduction to the complete calculation process. Graphene possesses a high breaking strength of $42\,\mathrm{Nm}^{-1}$ [23], thermal conductivity of $5 \times 10^3\,\mathrm{W/mK}$ [24], and electron transport mobility of over $2 \times 10^5\,\mathrm{cm^2V^{-1}s^{-1}}$ [25]. Graphene production ranges from simple mechanical exfoliation (peeling off 2D layers of graphene from a 3D graphite structure [26]) to more elaborate methods of chemical vapor deposition (where chemical reactions precipitate graphene onto a surface [27]). In biosensing, graphene has seen potential applications in nanopore (GNP) and nanoribbon (GNR) arrangements. As GNP, proposed methods involve measuring the ionic current across the pore as DNA passes through the 2D sheet [28], and as GNR, the current changes due to adsorption onto the surface [4]. As a preliminary look into graphene, this project will first analyze the adsorption of DNA nucleobases on the surface of a 2D graphene sheet.

4.1 Constructing Graphene Structure

Constructing a structure for graphene starts with the basic unit cell: two carbon atoms with a bond length of 1.42 Å at an angle of 30° with the x-axis, as seen in Fig. 4.1.

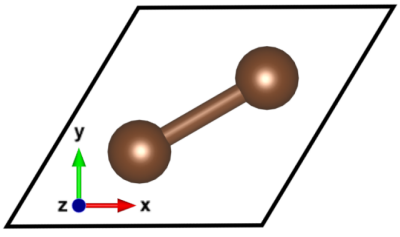

FIGURE 4.1: VESTA visualization of graphene unit cell.

This unit cell is repeated in the x- and y-directions to create a hexagonal structure, and this project uses a 5x5 arrangement of the unit cell, seen in Fig. 4.2. This constructed supercell has a width of 11.07 Å and a height of 9.23 Å, making it just large enough to hold each nucleobase without being unnecessarily large, which would increase computing time. The XYZ files were generated using a Python script that utilizes the *pandas* library to create a database containing all of the coordinates of each carbon atom.

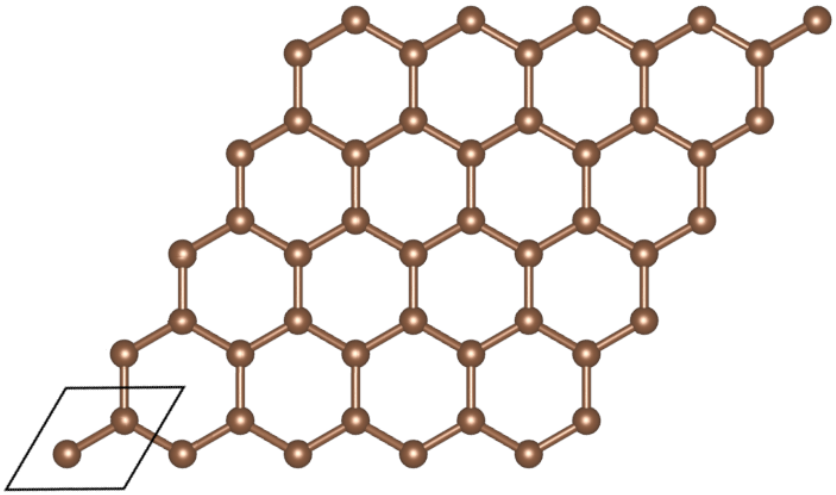

FIGURE 4.2: Graphene 5x5 supercell structure. Outlined in a black rhombus is the unit cell of the system.

4.2 Creating Input Files

After the graphene XYZ coordinate generation, a second Python script combines this information with each of the base XYZ files in an adsorption configuration. The script accomplishes this by first placing the geometric center of the graphene structure and each nucleobase structure about the origin $(0, 0, 0)$, then offsetting the z-coordinates of each atom in each nucleobase to create a desired distance. Performing *relax* calculations on the combined system produce optimized distances between the nucleobase and the graphene surface. Fig. 4.3 & 4.4 show the positioning of each base adsorbed on the graphene surface.

4.3 Performing Calculations

Like before with the nucleobases, we perform *relax* calculations on each of the systems to determine the optimized coordinates of each atom, followed by an *scf* calculation

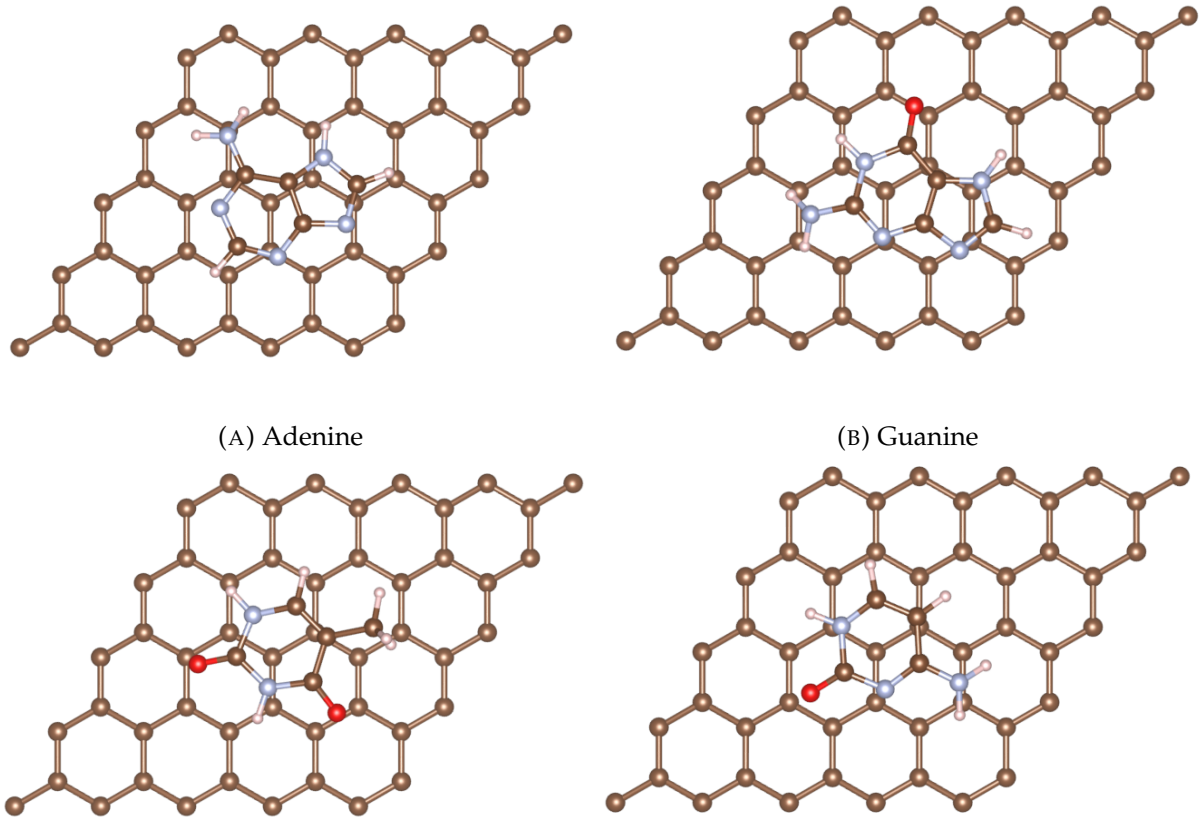

(A) Adenine (B) Guanine

(C) Thymine (D) Cytosine

FIGURE 4.3: Top view (looking down the z-axis) of each nucleobase held above the graphene surface.

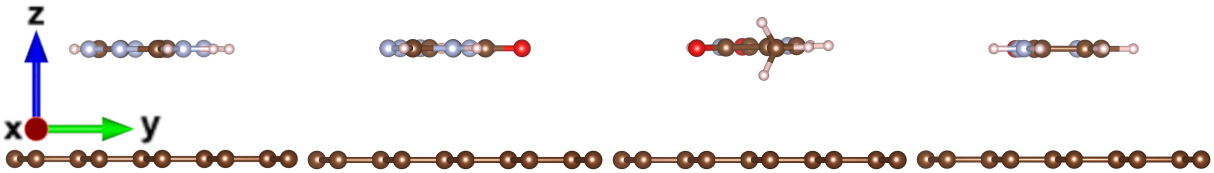

(A) Adenine (B) Guanine (C) Thymine (D) Cytosine

FIGURE 4.4: Side view (looking down the x-axis) of each nucleobase held above the graphene surface.

to find the total energies. Since the van der Waals force may affect the final vertical height and binding energy, we perform the sequence of calculations twice: once using just the PBE functional and once using PBE with a vdW correction. Following this, we calculate and plot the electronic band structure of each system to observe the effects of physisorption. The band structure (a 'fingerprint' of the system) displays the energy level of each electron as a function of its location in the lattice. In the process of plotting the band structures, we normalize each dataset by subtracting the Fermi energy, (E_F, defined as the difference in energy level between the highest and lowest occupied state states) from all of the energy levels. In the *scf* output file, QE helpfully writes the Fermi energy in eV:

```
the Fermi energy is    -3.4246 ev
```

4.4 Results

4.4.1 PBE

Performing *relax* calculations on the nucleobases interacting with the graphene allows each base to find an optimal distance above the surface where the system can reach its lowest total energy. We found regardless of where each base was placed near the graphene surface, the final positions settle into a state of physisorption shown in Fig. 4.5. In this case of utilizing just the PBE functional, the height ranges from 3.74 Å to 3.77 Å.

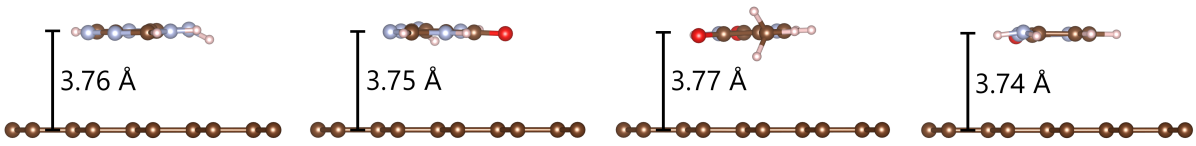

(A) Adenine (B) Guanine (C) Thymine (D) Cytosine

FIGURE 4.5: Final positions of DNA bases adsorbed onto the graphene surface using the PBE functional.

After the *relax* calculations find the final positions of each base, an *scf* calculation finds the total energy E_{tot} of the system. Looking back to Eq. 3.1, we subtract the parts of the system $E_{graphene}$ and E_{base} (also found using *scf* calculations) from the entire system to find the binding energy:

$$E_{tot} - (E_{graphene} + E_{base}) = E_{binding} \tag{4.1}$$

which gives us the binding energies shown in Table 4.1. Previous literature found that the relative values of the binding energies at approximately half an electronvolt [29], but using the PBE functional alone returns values an order of magnitude smaller.

TABLE 4.1: Graphene physisorption energy values (in eV) resulting from Fig. 4.5.

	E_{tot}	E_{graphene}	E_{base}	E_{binding}
Graphene + A	−10 749.3825	−8432.8099	−2316.4984	−0.0741
Graphene + G	−11 191.7829	−8432.8099	−2757.9075	−0.0654
Graphene + T	−10 813.2930	−8432.8099	−2380.4360	−0.0469
Graphene + C	−10 465.2222	−8432.8099	−2032.5055	−0.0828

4.4.2 PBE+vdW

When including the vdW correction, the final positions of the DNA bases contract to a range of 3.11 Å to 3.29 Å, as seen in Fig. 4.6. Like before, these positions correspond to binding energy values, and with the shorter height between the nucleobase and the graphene, more consistent with previously established values. In addition, the relative binding energy values of DNA nucleobases (G > A > C ∼ T) closely resemble a previously found order of G > A ∼ C ∼ T [29].

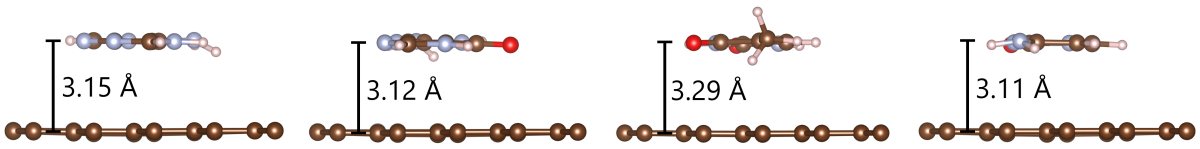

(A) Adenine (B) Guanine (C) Thymine (D) Cytosine

FIGURE 4.6: Final positions of DNA bases adsorbed onto the graphene surface using the PBE functional with a vdW correction.

Concluding with the bands calculation, the graphene band structure looks as expected, with the valence bands ($E - E_F > 0$) separate from the conduction bands ($E - E_F < 0$) at the Γ and M symmetry points and crossing at the K point [30]. With the introduction of nucleobase adsorption, the band structures shift slightly from that of pristine graphene, but the overall structure remains consistent.

TABLE 4.2: Graphene physisorption binding energies (in eV) resulting from Fig. 4.6.

	E_{tot}	E_{graphene}	E_{base}	E_{binding}
Graphene + A	−10 752.888	−8435.620	−2316.717	−0.550
Graphene + G	−11 194.367	−8435.620	−2758.158	−0.588
Graphene + T	−10 816.762	−8435.620	−2380.681	−0.461
Graphene + C	−10 468.588	−8435.620	−2032.505	−0.462

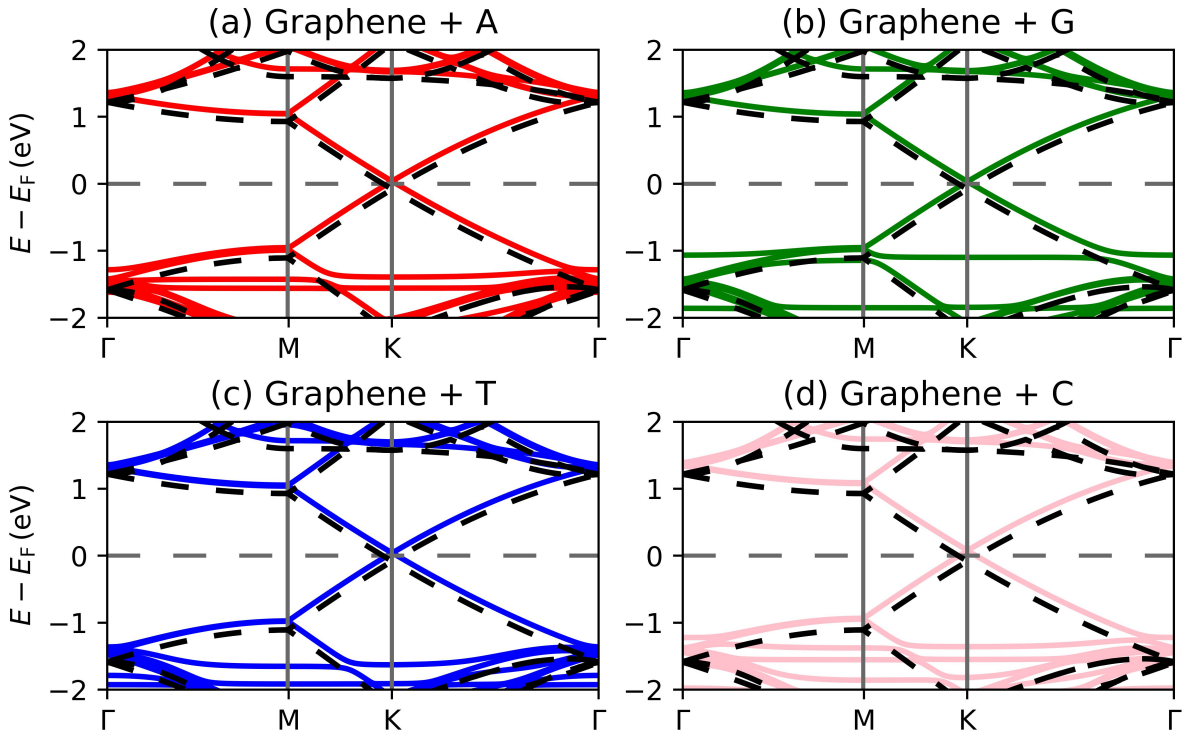

FIGURE 4.7: Band structures of graphene interacting with adsorbed nucleobases. The dashed black lines represent pristine graphene, while the solid colored lines represent the system after nucleobase adsorption.

Chapter 5

DNA Base Adsorption on Titanium Carbide MXene

Titanium carbide MXene has recently gained interest for its potential versatility in electrical and optical sensing technology. Ti_3C_2, being an MXene transition metal carbide, consists of alternating layers of transition metal (M_{n+1}) and carbon (X_n) [31]. Recent research has shown MXenes to have potential in a wide variety of applications, such as increasing the capacity of batteries [32], storing hydrogen[33], and adsorbing lead contaminants from water [34]. Ti_3C_2 in particular has been found to have graphene-like electronic stability [35] along with a hydrophilic surface [34]. This structure can be synthesized by starting with $Ti_{n+1}AlC_n$ powder and baked into a "MAX" bulk, which is then treated with hydrofluoric acid to etch out 2D MXene sheets to exfoliate [36].

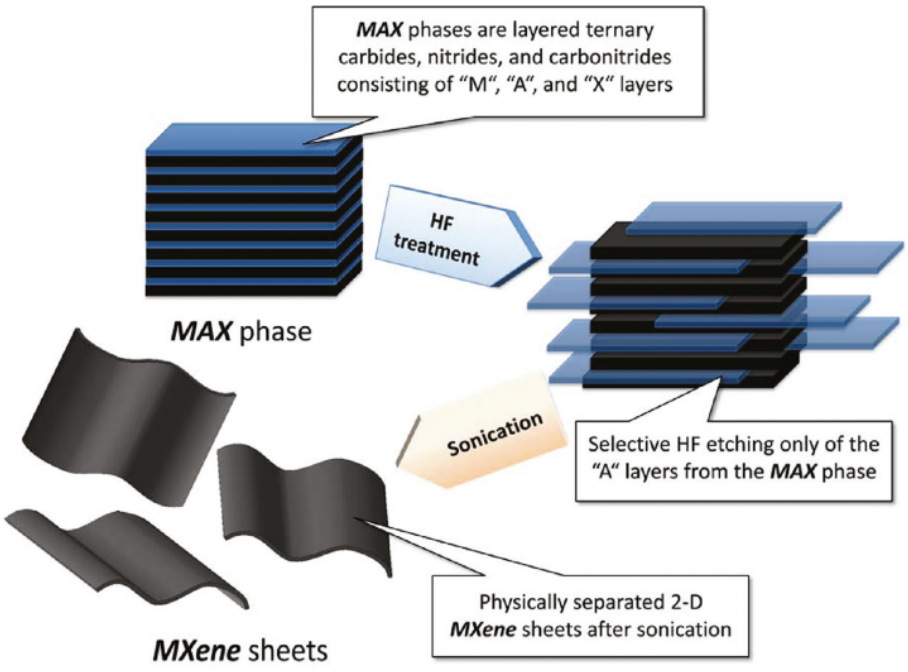

FIGURE 5.1: Overview of etching process to produce MXene sheets [31].

5.1 Constructing Titanium Carbide MXene Structure

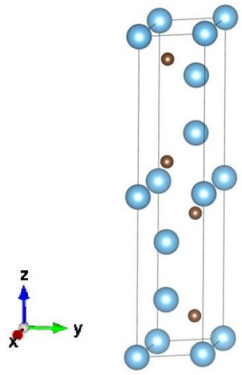

FIGURE 5.2: Conventional cell of the Ti_3C_2.

A single layer of Ti_3C_2 MXene consists of 5 alternating layers of titanium and carbon in a 3D hexagonal lattice structure. In the central layer, each titanium atom (Ti^{2+}) forms bonds of length 2.20 Å with six carbon atoms (C^{4-}) in the surrounding layers in an octahedral arrangement. Each titanium atom in the outer layers (Ti^{3+}) forms bonds of length 2.06 Å with three carbon atoms (C^{4-}) from the neighboring layer in a distorted T-shaped configuration [37]. Fig. 5.2 shows the conventional cell of the Ti_3C_2 MXene structure used to generate the full lattice structure.

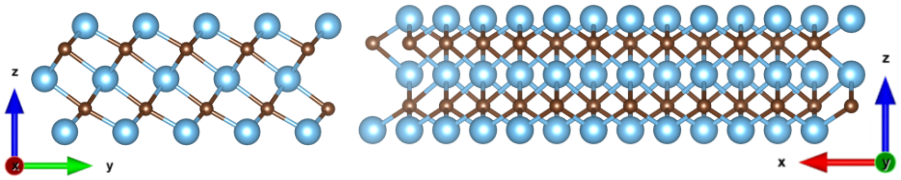

(A) Side view of Ti_3C_2, looking down the x-axis.

(B) Side view of Ti_3C_2, looking down the y-axis.

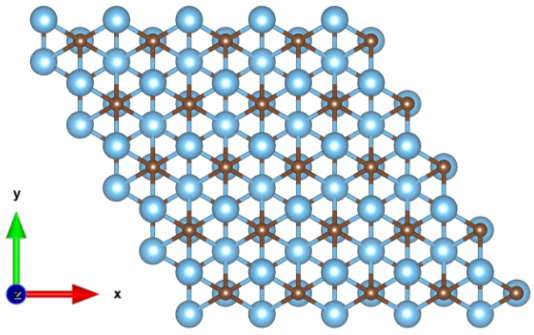

(C) Top view of Ti_3C_2, looking down the z-axis.

FIGURE 5.3: Ti_3C_2 structure used in adsorption computations.

5.2 Creating Input Files

Like before with graphene, generating the full structure of Ti_3C_2 requires a repeating the conventional cell in a 5x5 supercell arrangement, resulting in 75 titanium and 50 carbons atoms for a total of 125 atoms. The conventional cell repeated in the x- and y-directions creates the Ti_3C_2 surface shown in Fig. 5.3. With the Ti_3C_2 surface, each DNA base can be placed similarly to the method described in Section 4.2 with an additional consideration for how the base should be centered over the surface in the xy-directions. Since the MXene structure contains multiple layers of alternating elements, there exist the possibility of multiple stable configurations for the DNA base positions. To address this, two sets of the complete system were compiled: one with the main nitrogenous ring in the DNA base centered around a titanium atom in the top layer (shown in F.g 5.4), and the other with the ring structure centered around a carbon atom in the next-closest layer (shown in Fig. 5.5).

We found that the initial distance set between the DNA base and the MXene lattice can cause the base to adhere to the surface in two different ways: physisorption and chemisorption. In longer distances, above 5.5 Å, the optimized configuration results in adsorption mainly governed by the Van der Waals force. When the DNA base is brought to within 5.4 Å of the surface, electronic bonds form as the base chemically reacts with the titanium atoms.

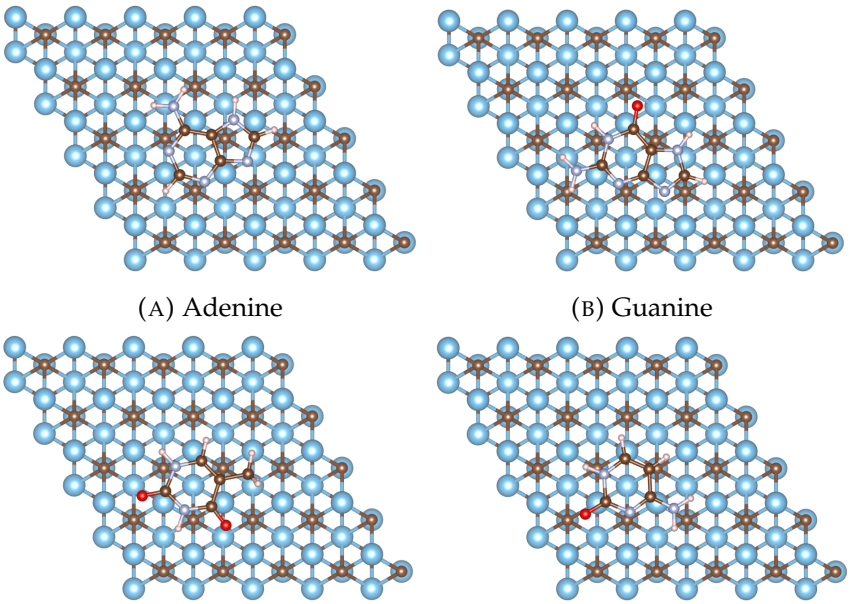

(A) Adenine (B) Guanine

(C) Thymine (D) Cytosine

FIGURE 5.4: Top view of nucleobases fixed over a top-layer titanium atom in Ti_3C_2.

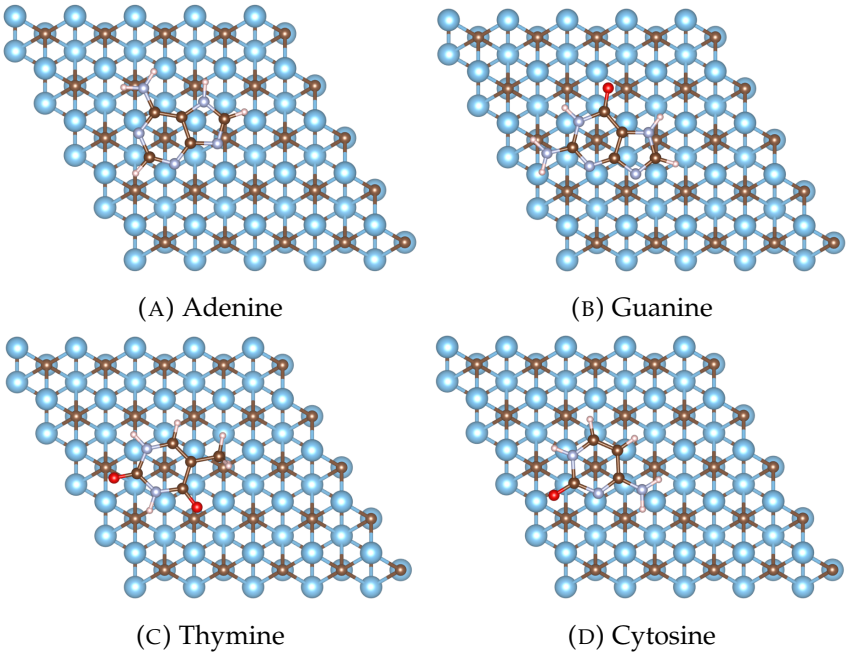

(A) Adenine (B) Guanine

(C) Thymine (D) Cytosine

FIGURE 5.5: Top view of nucleobases fixed over a second-layer carbon atom in Ti_3C_2.

5.3 Performing Calculations

Much like graphene, we first run *vc-relax* and *relax* calculations to determine the optimized unit cell dimensions and atomic coordinates. Once those aspects are determined, an *scf* calculation returns the total energy of the system and its Fermi energy. We repeat this process several times to account for all of the systems: PBE with titanium-centered bases and carbon-centered bases, and PBE+vdW with titanium-centered and carbon-centered bases. As previously done with graphene, we calculate the binding energy of each system by utilizing Eq. 3.1:

$$E_{\text{tot}} - (E_{Ti_3C_2} + E_{\text{base}}) = E_{\text{binding}} \tag{5.1}$$

In addition, with the detection of chemisorption in PBE+vdW calculations, we explore the effects of chemisorption on the final state of the system. Since Ti_3C_2 has the same 2D geometry as graphene, we can then use the same *babnds* process and symmetry points to calculate the band structures of the PBE+vdW systems.

5.4 Results

5.4.1 PBE

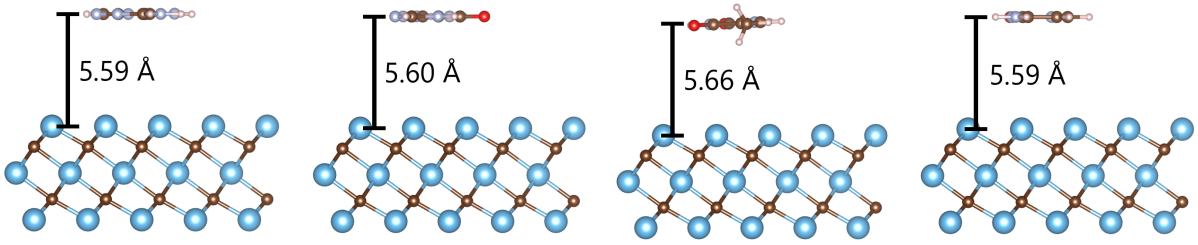

(A) Adenine (B) Guanine (C) Thymine (D) Cytosine

FIGURE 5.6: Final gap distances of nucleobases adsorbed onto the Ti_3C_2 surface.

In simple PBE calculations, both sets of systems (nucleobases oriented above a titanium atom or a carbon atom) returned the same final positions shown in Fig. 5.6, which range from 5.59 Å to 5.66 Å. A larger gaps between the nucleobases and the surface correlate to a smaller binding energy, which is seen in Tables 5.1 & 5.2. Centering the nucleobases over titanium or carbon had minimal effect on the binding energies, as the values differed by just thousandths of an electronvolt.

TABLE 5.1: PBE-derived Ti_3C_2 binding energies (in eV) resulting from titanium-centered nucleobases (Fig. 5.4).

	$E_{\mathbf{tot}}$	$E_{\mathbf{Ti_3C_2}}$	$E_{\mathbf{base}}$	$E_{\mathbf{binding}}$
Ti_3C_2 + A	−133 000.7922	−130 684.2401	−2316.4908	−0.0614
Ti_3C_2 + G	−133 442.1883	−130 684.2401	−2757.9082	−0.0400
Ti_3C_2 + T	−133 064.7338	−130 684.2401	−2380.4265	−0.0572
Ti_3C_2 + C	−132 716.6467	−130 684.2401	−2032.3292	−0.0775

TABLE 5.2: PBE-derived Ti_3C_2 binding energies (in eV) resulting from carbon-centered nucleobases (Fig. 5.5).

	$E_{\mathbf{tot}}$	$E_{\mathbf{Ti_3C_2}}$	$E_{\mathbf{base}}$	$E_{\mathbf{binding}}$
Ti_3C_2 + A	−133 000.7925	−130 684.2401	−2316.4908	−0.0616
Ti_3C_2 + G	−133 442.1888	−130 684.2401	−2757.9082	−0.0405
Ti_3C_2 + T	−133 064.7342	−130 684.2401	−2380.4265	−0.0577
Ti_3C_2 + C	−132 716.6474	−130 684.2401	−2032.3292	−0.0781

5.4.2 PBE+vdW

When taking into account the van der Waals force interactions around this gap distance, the Ti_3C_2 surface interacts with the nucleobases using two distinct mechanisms: physisorption and chemisorption. At distances above 5.5 Å, the nucleobases act in the same way as previously with just the PBE calculation. The final positions of the bases match those found in Fig. 5.6, though the binding energies (while still similar whether centered over titanium or carbon) increase substantially:

TABLE 5.3: PBE+vdW-derived Ti_3C_2 binding energies (in eV) resulting from titanium-centered nucleobases (Fig. 5.4).

	$E_{\mathbf{tot}}$	$E_{\mathbf{Ti_3C_2}}$	$E_{\mathbf{base}}$	$E_{\mathbf{binding}}$
Ti_3C_2 + A	−133 032.224	−130 715.340	−2316.709	−0.175
Ti_3C_2 + G	−133 473.658	−130 715.340	−2757.158	−0.161
Ti_3C_2 + T	−133 096.178	−130 715.340	−2380.681	−0.157
Ti_3C_2 + C	−132 748.015	−130 715.340	−2032.505	−0.169

TABLE 5.4: PBE+vdW-derived Ti_3C_2 binding energies (in eV) resulting from carbon-centered nucleobases (Fig. 5.5).

	$E_{\mathbf{tot}}$	$E_{\mathbf{Ti_3C_2}}$	$E_{\mathbf{base}}$	$E_{\mathbf{binding}}$
Ti_3C_2 + A	−133 032.224	−130 715.340	−2316.709	−0.175
Ti_3C_2 + G	−133 473.659	−130 715.340	−2757.158	−0.161
Ti_3C_2 + T	−133 096.178	−130 715.340	−2380.681	−0.158
Ti_3C_2 + C	−132 748.016	−130 715.340	−2032.505	−0.171

The band structures of the total system, again similarly to graphene, follow the structure of pristine Ti_3C_2 closely, with only minor deviations present across the nucleobases. The bands present in Fig. 5.7 do show more valence and conduction bands crossing the 0 eV energy level across the entire crystalline structure, indicating a more metallic surface where electrons have fewer restrictions on where they can easily flow.

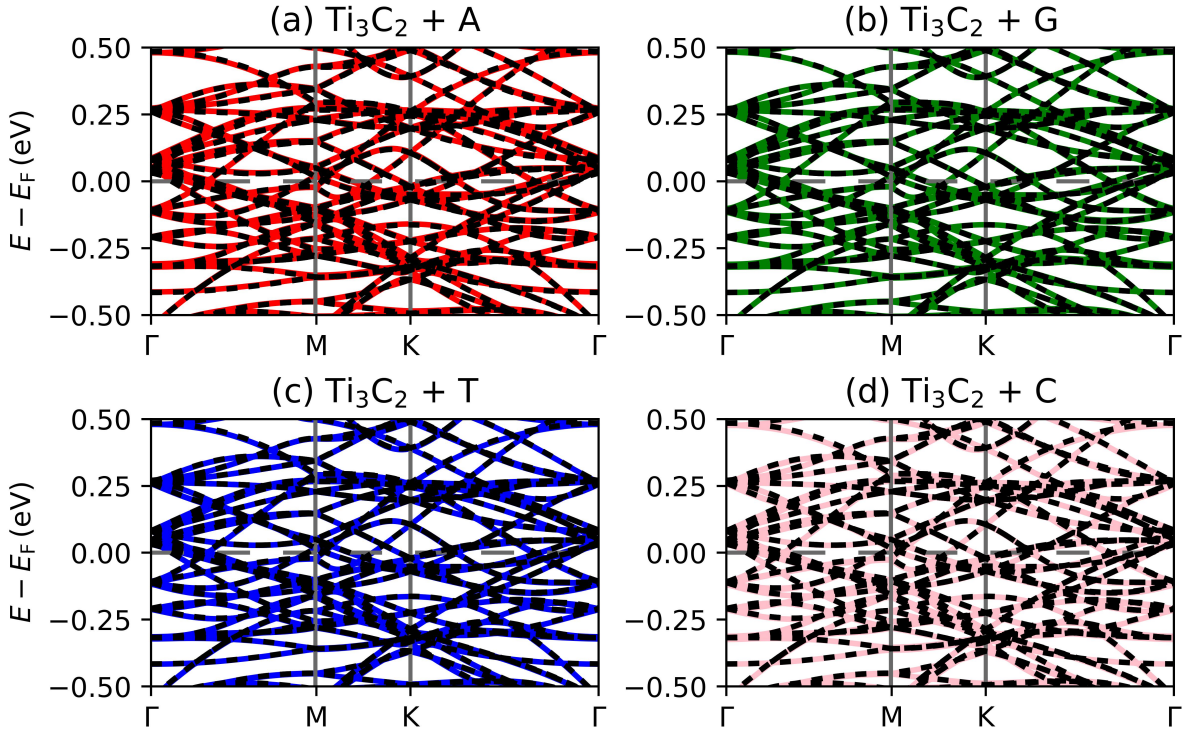

FIGURE 5.7: Band structures of DNA bases physisorbed on the Ti_3C_2 surface. The dashed black lines represent Ti_3C_2 on its own, while the solid colored lines represent the Ti_3C_2 surface after interacting with the nucleobase.

5.4.3 Chemisorption

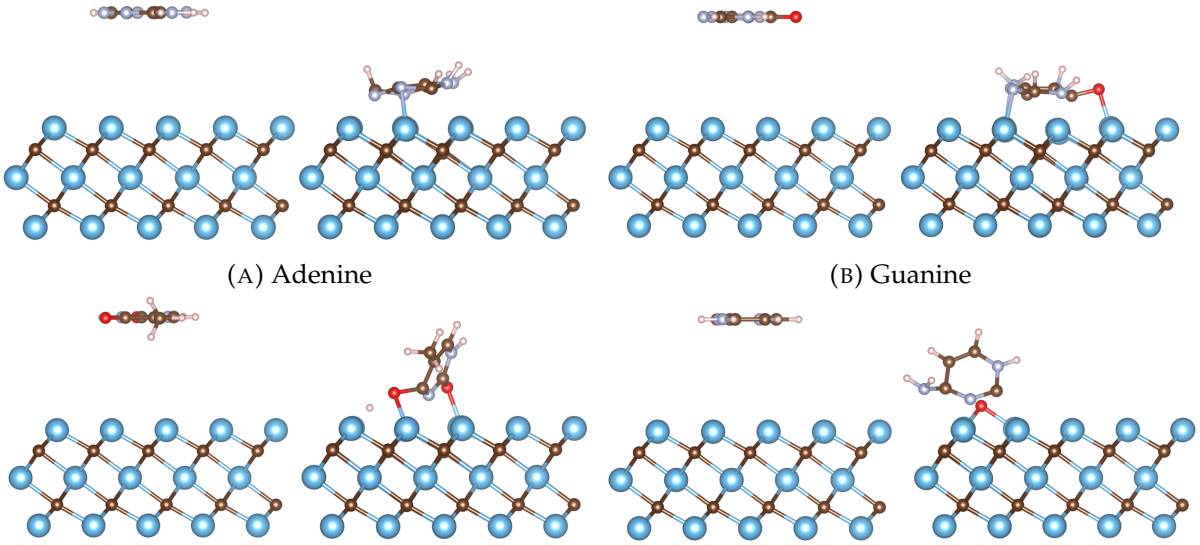

(A) Adenine (B) Guanine

(C) Thymine (D) Cytosine

FIGURE 5.8: DNA bases initially held at a distance of 5.4 Å above the surface engage in chemisorption. Each subfigure shows before (left) and after (right) performing *relax* calculations. Note that the purine nucleobases (adenine & guanine) adsorb parallel to the Ti_3C_2 surface, while the pyrimidine nucleobases (thymine & cytosine) adsorb approximately perpendicular to the surface.

When taking into account the vdW correction in the previous configuration, we noticed that within 5.4 Å of the Ti_3C_2 surface, the attractive intermolecular forces overcame any repulsive forces present and facilitated the formation of chemical bonds. The end results are seen in Fig. 5.8, where the nucleobases ended up in direct contact with the adsorption surface, and in the case of thymine and cytosine, the vdW force cause bonds to break in the nucleobase itself. Understandably, the resultant binding energies in Table 5.5 overshadow those found in with physisorption.

TABLE 5.5: Ti_3C_2 binding energies (in eV) resulting from chemisorption present in Fig. 5.8.

	$E_{\mathbf{tot}}$	$E_{\mathbf{Ti_3C_2}}$	$E_{\mathbf{base}}$	$E_{\mathbf{binding}}$
Ti_3C_2 + A	−133 038.77	−130 715.34	−2316.71	−6.72
Ti_3C_2 + G	−133 480.96	−130 715.34	−2757.16	−7.46
Ti_3C_2 + T	−133 101.89	−130 715.34	−2380.68	−5.87
Ti_3C_2 + C	−132 754.56	−130 715.34	−2032.51	−6.71

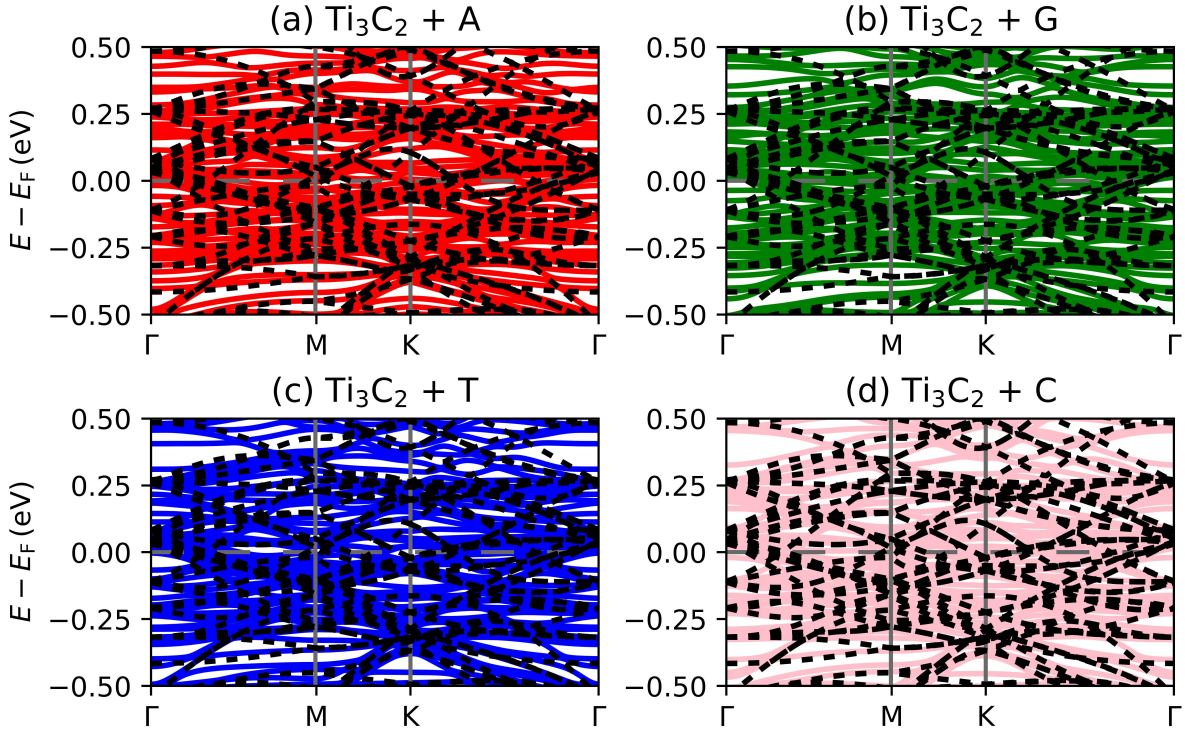

FIGURE 5.9: Band structures of nucleobases after undergoing chemisorption on the Ti_3C_2 surface. The dashed black lines represent pristine Ti_3C_2, while the solid colored lines represent the Ti_3C_2 surface after interacting with the nucleobase.

Since the new chemical bonds provide new paths for electrons to flow through, the band structures due to chemisorption depart radically from the pristine Ti_3C_2 bands. The system still retains its metallic properties, but the bands bear essentially no resemblance to the original structure.

Chapter 6

Conclusion

6.1 Summary of Results

Performing DFT calculations on graphene interacting with physisorbed DNA nucleobases returned results consistent with previous findings. By using the same methods on TiC, we found taller heights between itself and the nucleobases (Fig. 6.1), which correlate to smaller binding energies (Fig. 6.1). At first, the prospect of a material that possesses a lower risk of the DNA strand adhering to the surface, but we found that bringing the nucleotide any closer than 5.5 Å induces chemisorption. The resultant binding energies, also shown in Fig. 6.2, surpass the physisorption energies by an order of magnitude. This interaction would cause the DNA strand to be completely bonded to the Ti_3C_2 surface, likely rendering attempts at sequencing impossible. Therefore, according to our findings, while Ti_3C_2 may still have promising qualities for DNA sequencing, the adsorption difficulties do not make a Ti_3C_2 surface seem suitable for use in a nanoribbon configuration. However, the overall procedure we use should handle a variety of arrangements and materials.

6.2 Future Work

While our results did not indicate a viable adsorption surface, further studies could verify this outcome by investigating more complex systems, such as DNA nucleobases with attached methyl groups or even linked together into small chains with ribose sugars and phosphate groups. The main limitation of this study was the use of the DNA nucleobases as discrete structures, as opposed to their natural state as part of a strand. More comprehensive research would use more computing power, but should more accurately simulate the interactions present in real-world scenarios. Alternatively, since adsorption may be non-viable due to the chance of chemisorption, a nanopore configuration may prove more ideal. Future projects in this field of study at the University of Central Oklahoma could build off of the process outlined in this paper to delve deeper into the viability of Ti_3C_2 or other materials in a straightforward manner with results that are simple to compare. [38]

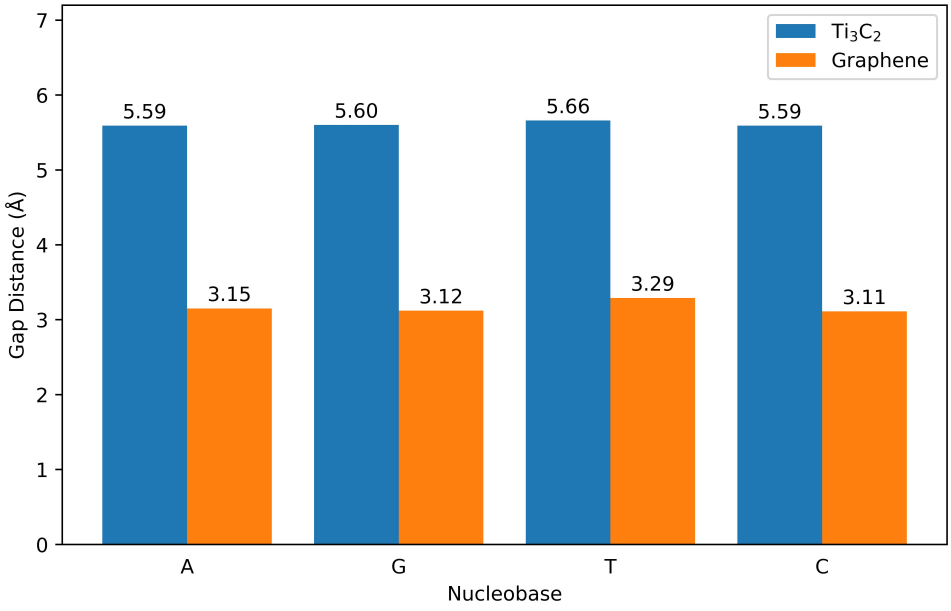

FIGURE 6.1: Bar plot of physisorption height values from Fig. 4.5 and Fig. 5.6.

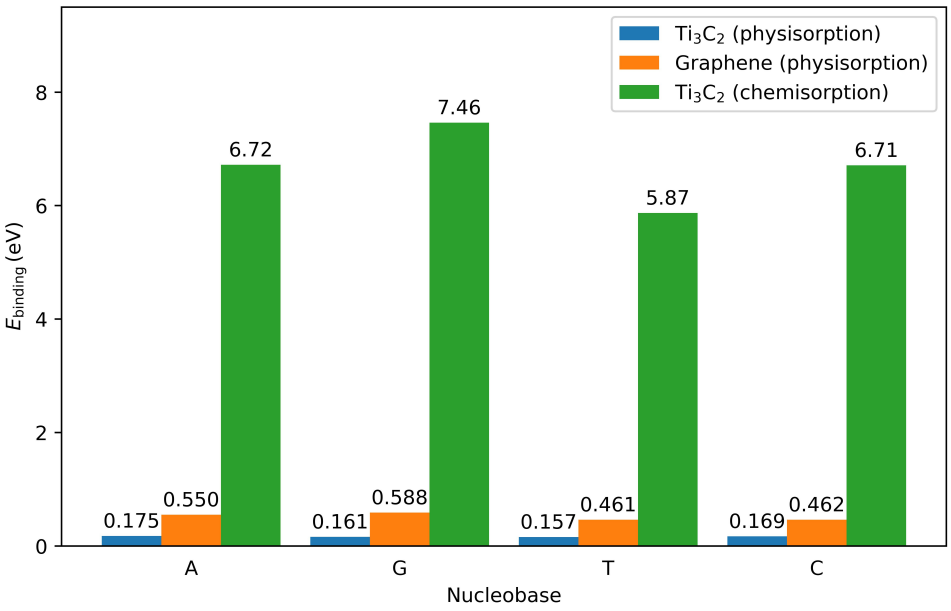

FIGURE 6.2: Bar plot of binding energy values between surface and nucleobases from Tables 4.2, 5.3, & 5.5.

Bibliography

[1] Jariyanee Prasongkit et al. "Transverse Conductance of DNA Nucleotides in a Graphene Nanogap from First Principles". In: *Nano Letters* 11.5 (May 2011), pp. 1941–1945. DOI: 10.1021/nl200147x. URL: https://doi.org/10.1021%2Fnl200147x.

[2] James M. Heather and Benjamin Chain. "The sequence of sequencers: The history of sequencing DNA". In: *Genomics* 107.1 (Jan. 2016), pp. 1–8. DOI: 10.1016/j.ygeno.2015.11.003. URL: https://doi.org/10.1016%2Fj.ygeno.2015.11.003.

[3] Wilhelm J. Ansorge. "Next-generation DNA sequencing techniques". In: *New Biotechnology* 25.4 (Apr. 2009), pp. 195–203. DOI: 10.1016/j.nbt.2008.12.009. URL: https://doi.org/10.1016%2Fj.nbt.2008.12.009.

[4] Stephanie J. Heerema and Cees Dekker. "Graphene nanodevices for DNA sequencing". In: *Nature Nanotechnology* 11.2 (Feb. 2016), pp. 127–136. DOI: 10.1038/nnano.2015.307. URL: https://doi.org/10.1038%2Fnnano.2015.307.

[5] Juan José Palacios. "Electrons go ballistic". In: *Nature Physics* 10.3 (Feb. 2014), pp. 182–183. DOI: 10.1038/nphys2909. URL: https://doi.org/10.1038%2Fnphys2909.

[6] Amir Barati Farimani, Kyoungmin Min, and Narayana R. Aluru. "DNA Base Detection Using a Single-Layer MoS_2". In: *ACS Nano* 8.8 (July 2014), pp. 7914–7922. DOI: 10.1021/nn5029295. URL: https://doi.org/10.1021%2Fnn5029295.

[7] Rameshwar L. Kumawat and Biswarup Pathak. "Individual Identification of DNA Nucleobases on Atomically Thin Black Phosphorene Nanoribbons: van der Waals Corrected Density Functional Theory Calculations". In: *The Journal of Physical Chemistry C* 123.36 (Aug. 2019), pp. 22377–22383. DOI: 10.1021/acs.jpcc.9b06239. URL: https://doi.org/10.1021%2Facs.jpcc.9b06239.

[8] Jacob K Rosenstein et al. "Integrated nanopore sensing platform with submicrosecond temporal resolution". In: *Nature Methods* 9.5 (Mar. 2012), pp. 487–492. DOI: 10.1038/nmeth.1932. URL: https://doi.org/10.1038%2Fnmeth.1932.

[9] Jürg Riess and Walter Münch. "The theorem of hohenberg and kohn for subdomains of a quantum system". In: *Theoretica Chimica Acta* 58.4 (Apr. 1981), pp. 295–300. DOI: 10.1007/bf02426905. URL: https://doi.org/10.1007%2Fbf02426905.

[10] Dmitrij Rappoport et al. *Approximate Density Functionals: Which Should I Choose?* Sept. 2009. DOI: 10.1002/0470862106.ia615. URL: https://doi.org/10.1002%2F0470862106.ia615.

[11] Mark T. Lusk and Ann E. Mattsson. "High-performance computing for materials design to advance energy science". In: *MRS Bulletin* 36.3 (Mar. 2011), pp. 169–174. DOI: 10.1557/mrs.2011.30. URL: https://doi.org/10.1557%2Fmrs.2011.30.

[12] J. C. Slater. "A Simplification of the Hartree-Fock Method". In: *Physical Review* 81.3 (Feb. 1951), pp. 385–390. DOI: 10.1103/physrev.81.385. URL: https://doi.org/10.1103%2Fphysrev.81.385.

[13] Per-Olov Löwdin. "Quantum Theory of Many-Particle Systems. III. Extension of the Hartree-Fock Scheme to Include Degenerate Systems and Correlation Effects". In: *Physical Review* 97.6 (Mar. 1955), pp. 1509–1520. DOI: 10.1103/physrev.97.1509. URL: https://doi.org/10.1103%2Fphysrev.97.1509.

[14] John P. Perdew, Kieron Burke, and Matthias Ernzerhof. "Generalized Gradient Approximation Made Simple". In: *Physical Review Letters* 77.18 (Oct. 1996), pp. 3865–3868. DOI: 10.1103/physrevlett.77.3865. URL: https://doi.org/10.1103%2Fphysrevlett.77.3865.

[15] Matthew B. Henry. "A Computational Study of Graphene and Phosphorene for DNA Base Detection". MS Thesis. University of Central Oklahoma, Dec. 2020. URL: https://shareok.org/handle/11244/330111.

[16] *Input file description*. URL: https://www.quantum-espresso.org/Doc/INPUT_PW.html.

[17] "van der Waals forces". In: *The IUPAC Compendium of Chemical Terminology*. International Union of Pure and Applied Chemistry (IUPAC), Feb. 2014. DOI: 10.1351/goldbook.v06597. URL: https://doi.org/10.1351%2Fgoldbook.v06597.

[18] Stefan Grimme. "Semiempirical GGA-type density functional constructed with a long-range dispersion correction". In: *Journal of Computational Chemistry* 27.15 (2006), pp. 1787–1799. DOI: 10.1002/jcc.20495. URL: https://doi.org/10.1002/jcc.20495.

[19] Tomáš Bučko et al. "Improved Description of the Structure of Molecular and Layered Crystals: Ab Initio DFT Calculations with van der Waals Corrections". In: *The Journal of Physical Chemistry A* 114.43 (Oct. 2010), pp. 11814–11824. DOI: 10.1021/jp106469x. URL: https://doi.org/10.1021%2Fjp106469x.

[20] Wahyu Setyawan and Stefano Curtarolo. "High-throughput electronic band structure calculations: Challenges and tools". In: *Computational Materials Science* 49.2 (Aug. 2010), pp. 299–312. DOI: 10.1016/j.commatsci.2010.05.010. URL: https://doi.org/10.1016%2Fj.commatsci.2010.05.010.

[21] Sona Sivakova and Stuart J. Rowan. "Nucleobases as supramolecular motifs". In: *Chemical Society Reviews* 34.1 (2005), p. 9. DOI: 10.1039/b304608g. URL: https://doi.org/10.1039%2Fb304608g.

[22] *Rydberg constant times hc in eV*. URL: https://physics.nist.gov/cgi-bin/cuu/Value?rydhcev.

[23] Changgu Lee et al. "Measurement of the Elastic Properties and Intrinsic Strength of Monolayer Graphene". In: *Science* 321.5887 (July 2008), pp. 385–388. DOI: 10.1126/science.1157996. URL: https://doi.org/10.1126%2Fscience.1157996.

[24] Alexander A. Balandin et al. "Superior Thermal Conductivity of Single-Layer Graphene". In: *Nano Letters* 8.3 (Feb. 2008), pp. 902–907. DOI: 10.1021/nl0731872. URL: https://doi.org/10.1021%2Fnl0731872.

[25] Phaedon Avouris. "Graphene: Electronic and Photonic Properties and Devices". In: *Nano Letters* 10.11 (Sept. 2010), pp. 4285–4294. DOI: 10.1021/nl102824h. URL: https://doi.org/10.1021%2Fnl102824h.

[26] K. S. Novoselov et al. "Electric Field Effect in Atomically Thin Carbon Films". In: *Science* 306.5696 (Oct. 2004), pp. 666–669. DOI: 10.1126/science.1102896. URL: https://doi.org/10.1126%2Fscience.1102896.

[27] Yi Zhang, Luyao Zhang, and Chongwu Zhou. "Review of Chemical Vapor Deposition of Graphene and Related Applications". In: *Accounts of Chemical Research* 46.10 (Mar. 2013), pp. 2329–2339. DOI: 10.1021/ar300203n. URL: https://doi.org/10.1021%2Far300203n.

[28] Grégory F. Schneider et al. "DNA Translocation through Graphene Nanopores". In: *Nano Letters* 10.8 (July 2010), pp. 3163–3167. DOI: 10.1021/nl102069z. URL: https://doi.org/10.1021%2Fnl102069z.

[29] Jun-Ho Lee et al. "Physisorption of DNA Nucleobases on *h*-BN and Graphene: vdW-Corrected DFT Calculations". In: *The Journal of Physical Chemistry C* 117.26 (June 2013), pp. 13435–13441. DOI: 10.1021/jp402403f. URL: https://doi.org/10.1021%2Fjp402403f.

[30] E. Kogan and V. U. Nazarov. "Symmetry classification of energy bands in graphene". In: *Physical Review B* 85.11 (Mar. 2012). DOI: 10.1103/physrevb.85.115418. URL: https://doi.org/10.1103%2Fphysrevb.85.115418.

[31] Johnson Michael, Zhang Qifeng, and Wang Danling. "Titanium carbide MXene: Synthesis, electrical and optical properties and their applications in sensors and energy storage devices". In: *Nanomaterials and Nanotechnology* 9 (Jan. 2019), pp. 1–9. DOI: 10.1177/1847980418824470. URL: https://doi.org/10.1177%2F1847980418824470.

[32] Michael Naguib et al. "MXene: a promising transition metal carbide anode for lithium-ion batteries". In: *Electrochemistry Communications* 16.1 (Mar. 2012), pp. 61–64. DOI: 10.1016/j.elecom.2012.01.002. URL: https://doi.org/10.1016%2Fj.elecom.2012.01.002.

[33] Qianku Hu et al. "MXene: A New Family of Promising Hydrogen Storage Medium". In: *The Journal of Physical Chemistry A* 117.51 (Dec. 2013), pp. 14253–14260. DOI: 10.1021/jp409585v. URL: https://doi.org/10.1021%2Fjp409585v.

[34] Qiuming Peng et al. "Unique Lead Adsorption Behavior of Activated Hydroxyl Group in Two-Dimensional Titanium Carbide". In: *Journal of the American Chemical Society* 136.11 (Mar. 2014), pp. 4113–4116. DOI: 10.1021/ja500506k. URL: https://doi.org/10.1021%2Fja500506k.

[35] I.R. Shein and A.L. Ivanovskii. "Graphene-like titanium carbides and nitrides $Ti_{n+1}C_n$, $Ti_{n+1}N_n$ (n=1, 2, and 3) from de-intercalated MAX phases: First-principles probing of their structural, electronic properties and relative stability". In: *Computational Materials Science* 65 (Dec. 2012), pp. 104–114. DOI: 10.1016/j.commatsci.2012.07.011. URL: https://doi.org/10.1016%2Fj.commatsci.2012.07.011.

[36] Aihu Feng et al. "Two-dimensional MXene Ti_3C_2 produced by exfoliation of Ti_3AlC_2". In: *Materials & Design* 114 (Jan. 2017), pp. 161–166. DOI: 10.1016/j.matdes.2016.10.053. URL: https://doi.org/10.1016%2Fj.matdes.2016.10.053.

[37] *Data retrieved from the Materials Project for Ti3C2 (mp-1094034) from database version v2022.10.28.* URL: https://materialsproject.org/materials/mp-1094034/.

[38] Prakarsh Yadav, Zhonglin Cao, and Amir Barati Farimani. "DNA Detection with Single-Layer Ti_3C_2 MXene Nanopore". In: *ACS Nano* 15.3 (Mar. 2021), pp. 4861–4869. DOI: 10.1021/acsnano.0c09595. URL: https://doi.org/10.1021%2Facsnano.0c09595.

Appendix A

Sample Input File

```
&CONTROL
    calculation  = ‘relax’ ,
    restart_mode = ‘from_scratch’ ,
    pseudo_dir = ‘./’ ,
    outdir = ‘./outdir’ ,
    prefix = ‘2DTiC-relax-pbe-vdW’ ,
    tstress = .true. ,
    tprnfor = .true. ,
    nstep = 500
/
&SYSTEM
    ecutwfc = 45.0 ,
    ecutrho = 450.0 ,
    occupations = ‘smearing’ ,
    degauss = 0.005 ,
    vdw_corr = ‘Grimme-D2’ ,
    ibrav = 4 ,
    celldm(1) = 29.15177719 ,
    celldm(3) = 1.96 ,
    nat = 140 ,
    ntyp = 4 ,
    lspinorb = .false.
/
&ELECTRONS
    diagonalization = ‘david’ ,
    mixing_mode = ‘plain’ ,
    conv_thr = 1.0d-5 ,
    mixing_beta = 0.05 ,
    electron_maxstep = 500
/
&IONS
/
```

```
&CELL
/
ATOMIC_SPECIES
H   1.0078   H.pbe-rrkjus_psl.1.0.0.UPF
C   12.0107  C.pbe-n-rrkjus_psl.1.0.0.UPF
N   14.006   N.pbe-n-rrkjus_psl.1.0.0.UPF
Ti  47.8670  Ti.pbe-spn-rrkjus_psl.1.0.0.UPF

ATOMIC_POSITIONS crystal
Ti  -3.8612499059   -6.2420646236   -0.0000052776
Ti  -2.3168407324   -5.3503021026   -2.3222391397
Ti  -3.8611679970   -4.4586819503   2.3222430090
C   -3.8613802717   -4.4586536504   -1.3133022756
C   -2.3167152723   -5.3504611543   1.3132424691
Ti  -5.4059201237   -3.5668331256   0.0001264744
Ti  -3.8613412275   -2.6752687776   -2.3222713632
Ti  -5.4056663004   -1.7834033602   2.3222619169
C   -5.4058372291   -1.7835932991   -1.3133399505
C   -3.8612768977   -2.6752090384   1.3132526364
Ti  -6.9503143840   -0.8917210766   0.0000213363
Ti  -5.4056511393   -0.0003170029   -2.3224091219
Ti  -6.9499726392   0.8917076156    2.3220525807
C   -6.9501325829   0.8914747725    -1.3135951915
C   -5.4056115662   -0.0000922476   1.3130401007
Ti  -8.4946065015   1.7833447307    -0.0002207608
Ti  -6.9499848850   2.6748422609    -2.3225964054
Ti  -8.4942892558   3.5666614252    2.3219474214
C   -8.4944905781   3.5666197269    -1.3137666985
C   -6.9499177290   2.6749728745    1.3128240324
Ti  -10.0390177485  4.4584805904    -0.0002415571
Ti  -8.4945265282   5.3501661779    -2.3224652975
Ti  -10.0388475514  6.2417553207    2.3219513035
C   -10.0390988122  6.2419145323    -1.3136349023
C   -8.4944160386   5.3500386260    1.3128603182
Ti  -0.7721058106   -6.2421699797   -0.0001410457
Ti  0.7722603912    -5.3502231798   -2.3222721978
Ti  -0.7722649145   -4.4587360873   2.3222802188
C   -0.7722645267   -4.4586544510   -1.3133224345
C   0.7721831010    -5.3504617028   1.3132619668
Ti  -2.3167655589   -3.5669369720   -0.0000066070
Ti  -0.7722270018   -2.6751979269   -2.3222910707
Ti  -2.3167600064   -1.7834558404   2.3222826541
```

```
C   -2.3167123974   -1.7835974497   -1.3133550689
C   -0.7723789562   -2.6752096539   1.3132780255
Ti  -3.8611500266   -0.8918308658   -0.0001080984
Ti  -2.3165251192   -0.0002505899   -2.3224205695
Ti  -3.8610684414   0.8916546330    2.3220725355
C   -3.8610114382   0.8914739731    -1.3136162151
C   -2.3167108507   -0.0000940002   1.3130581627
Ti  -5.4054555582   1.7832384865    -0.0003620697
Ti  -3.8608613217   2.6749125363    -2.3226149251
Ti  -5.4053824175   3.5666019108    2.3219700795
C   -5.4053669945   3.5666182178    -1.3137918659
C   -3.8610165526   2.6749697526    1.3128346309
Ti  -6.9498723327   4.4583725222    -0.0003760264
Ti  -5.4054143018   5.3502408709    -2.3224905000
Ti  -6.9499509575   6.2417041738    2.3219837717
C   -6.9499859241   6.2419170048    -1.3136700439
C   -5.4055196364   5.3500346225    1.3128799852
Ti  2.3167988392    -6.2420942577   -0.0000461533
Ti  3.8611283397    -5.3500703484   -2.3220639389
Ti  2.3164567655    -4.4586626281   2.3224164272
C   2.3166212801    -4.4585208477   -1.3131149333
C   3.8610030034    -5.3503226488   1.3135038710
Ti  0.7721314842    -3.5668523629   0.0000851511
Ti  2.3166356531    -2.6750470619   -2.3220922253
Ti  0.7719625092    -1.7833853333   2.3224187489
C   0.7721776013    -1.7834642107   -1.3131442166
C   2.3164445871    -2.6750745875   1.3135254959
Ti  -0.7722468268   -0.8917563692   -0.0000133851
Ti  0.7723425194    -0.0000985829   -2.3222120870
Ti  -0.7723421697   0.8917294459    2.3221997280
C   -0.7721132217   0.8915999226    -1.3133939256
C   0.7721110097    0.0000413177    1.3133096473
Ti  -2.3165455804   1.7833058270    -0.0002659110
Ti  -0.7719790900   2.6750555897    -2.3224034956
Ti  -2.3166568731   3.5666740703    2.3220982237
C   -2.3164732153   3.5667464375    -1.3135737384
C   -0.7721929909   2.6751087352    1.3130767132
Ti  -3.8609690177   4.4584495504    -0.0002905013
Ti  -2.3165357597   5.3503839115    -2.3222754376
Ti  -3.8612217298   6.2417728823    2.3221080162
C   -3.8610895953   6.2420479256    -1.3134574327
C   -2.3166954274   5.3501712038    1.3131157811
```

```
Ti  5.4056189960    -6.2419582171   0.0001928945
Ti  6.9498535838    -5.3500228675   -2.3219478329
Ti  5.4053723982    -4.4585141733   2.3225980449
C   5.4054466343    -4.4583948591   -1.3128860289
C   6.9499181522    -5.3502081272   1.3136681184
Ti  3.8609470303    -3.5667202296   0.0003318571
Ti  5.4053488401    -2.6749892058   -2.3219915393
Ti  3.8608762457    -1.7832391693   2.3226149251
C   3.8609942445    -1.7833362094   -1.3129207123
C   5.4053570346    -2.6749560835   1.3136873859
Ti  2.3165622206    -0.8916208011   0.0002290675
Ti  3.8610567171    -0.0000436079   -2.3221179270
Ti  2.3165655377    0.8918758919    2.3223982058
C   2.3167097308    0.8917272887    -1.3131678849
C   3.8610235556    0.0001578586    1.3134870828
Ti  0.7722736161    1.7834340033    -0.0000173993
Ti  2.3167357884    2.6751094504    -2.3222987855
Ti  0.7722542773    3.5668232432    2.3222924338
C   0.7723573180    3.5668692093    -1.3133340136
C   2.3167208979    2.6752244584    1.3132609018
Ti  -0.7721452977   4.4585827645    -0.0000408823
Ti  0.7721898474    5.3504307906    -2.3221671471
Ti  -0.7723085682   6.2419205474    2.3222904273
C   -0.7722630321   6.2421699798    -1.3132219274
C   0.7722198879    5.3502886440    1.3132845855
Ti  8.4945688475    -6.2418951058   0.0002237305
Ti  10.0388421695   -5.3501132917   -2.3219379991
Ti  8.4945329526    -4.4584734592   2.3224702246
C   8.4943662812    -4.4584469306   -1.3129154570
C   10.0390988122   -5.3502391431   1.3135686947
Ti  6.9498920721    -3.5666631513   0.0003533302
Ti  8.4943344400    -2.6750788067   -2.3219813224
Ti  6.9500388306    -1.7831982214   2.3224941945
C   6.9499104308    -1.7833901103   -1.3129522043
C   8.4945364365    -2.6749856765   1.3135825409
Ti  5.4055026431    -0.8915549145   0.0002585071
Ti  6.9500304062    -0.0001290650   -2.3221170512
Ti  5.4057291690    0.8919144072    2.3222814984
C   5.4056194260    0.8916816984    -1.3132061538
C   6.9502002255    0.0001306917    1.3133792800
Ti  3.8612174046    1.7835029995    0.0000096237
Ti  5.4057045020    2.6750288727    -2.3222984756
```

```
Ti  3.8614153665    3.5668674951    2.3221784066
C   3.8612697053    3.5668204530    -1.3133651184
C   5.4058984456    2.6751947220    1.3131648863
Ti  2.3168059501    4.4586486233    -0.0000107872
Ti  3.8611721562    5.3503428881    -2.3221603749
Ti  2.3168504094    6.2419590335    2.3221707183
C   2.3166578052    6.2421178935    -1.3132523825
C   3.8614008840    5.3502597957    1.3131957588
N   -2.1148878842   -0.6688743314   7.9168268989
C   -1.5645848371   -1.9014789983   7.9145908342
N   -0.2747851247   -2.2393473247   7.9148100384
C   0.5471994438    -1.1716011014   7.9169010596
N   1.9320782589    -1.2009400242   7.9162650037
C   2.2930056916    0.0645058718    7.9183816696
N   1.2324261969    0.9434755989    7.9217341268
C   0.0862936652    0.1624782511    7.9200987670
C   -1.2993550872   0.3978109920    7.9213603962
N   -1.8768733512   1.6345310611    7.9330623563
H   -2.2814712066   -2.7258551519   7.9129594353
H   3.3188951748    0.4214284331    7.9174398315
H   1.3025179221    1.9549871335    7.9182719605
H   -1.3420031222   2.4895812751    7.9121674941
H   -2.8883182396   1.6810464713    7.9147496378

K_POINTS automatic
1 1 1 0 0 0
```

Appendix B

Sample XYZ file

```
15
#Adenine PBE optimized by Dr. Tayo
N              8.3536029491         7.2940624582         2.8989655983
C              8.9039059962         6.0614577913         2.8967295336
N             10.1937057087         5.7235894649         2.8969487378
C             11.0156902772         6.7913356882         2.8990397590
N             12.4005690923         6.7619967654         2.8984037031
C             12.7614965250         8.0274426614         2.9005203690
N             11.7009170303         8.9064123885         2.9038728262
C             10.5547844986         8.1254150407         2.9022374664
C              9.1691357462         8.3607477816         2.9034990956
N              8.5916174822         9.5974678507         2.9152010557
H              8.1870196268         5.2370816377         2.8950981347
H             13.7873860082         8.3843652227         2.8995785309
H             11.7710087554         9.9179239231         2.9004106599
H              9.1264877112        10.4525180647         2.8943061935
H              7.5801725937         9.6439832609         2.8968883372
```

Appendix C

Sample Batch Script

```
#!/bin/bash
#
#SBATCH --partition=general
#SBATCH --nodes=4
#SBATCH --ntasks=80
#SBATCH --ntasks-per-node=20
#SBATCH --output=myoutput-%j.txt
#SBATCH --error=QEerr-%j.txt
#SBATCH --exclusive
#SBATCH --time=48:00:00
#SBATCH --job-name=pwscf
#SBATCH --mail-user=mwalkup5@uco.edu
#SBATCH --mail-type=ALL

module load QuantumESPRESSO
mpirun pw.x -in relax.in > relax.out


date
time \
```

Appendix D

Scholarly Presentations

1. Michael A. Walkup and Benjamin O. Tayo, "Interaction of DNA Bases with Single-Layer Ti_3C_2 MXene Nanoribbon: First-Principle Studies," Joint Fall 2022 Meeting of the Texas Section of the APS, Texas Section of the AAPT, and Zone 13 of the SPS, Poster Presentation, October 14, 2022

2. Michael A. Walkup and Benjamin O. Tayo, "Interaction of DNA Bases with Single-Layer Ti_3C_2 MXene Nanoribbon," Oklahoma Research Day, Poster Presentation, March 3, 2023

3. Benjamin O. Tayo, Michael A. Walkup, Sanjiv Jha, and Chinedu Ekuma, "Detection of DNA Bases Using Single-Layer Ti_3C_2 MXene: Density Functional Calculations," Bulletin of the American Physical Society, Oral Presentation, 2023